Densely integrated microring resonator based photonic devices for use in access networks

Edwin J. Klein[1*], Patryk Urban[2], Gabriel Sengo[1], Lucy T. H. Hilderink[1], Marcel Hoekman[1], Rudy Pellens[3], Paul van Dijk[3] and Alfred Driessen[1]

[1]Integrated Optical Micro Systems, MESA+ Research Institute, University of Twente, P.O.Box 217, 7500 AE Enschede, The Netherlands
[2]Cobra Research Institute, Eindhoven University of Technology, P.O. Box 513, 5600 MB Eindhoven, The Netherlands
[3]ASML Netherlands B.V., Veldhoven, The Netherlands
[*]e.j.klein@utwente.nl

Abstract: Two reconfigurable optical add-drop multiplexers, operating in the second or third telecom window, as well as a 1x4x4 reconfigurable λ-router operating in the second telecom window, are demonstrated. The devices have a footprint less than 2 mm^2 and are based on thermally tunable vertically coupled microring resonators fabricated in Si_3N_4/SiO_2.

©2007 Optical Society of America

OCIS codes: (060.1810) Couplers, switches, and multiplexers; (130.3120) Integrated optics devices.

References

1. T. Koonen, "Fiber to the Home/Fiber to the Premises: What, Where, and When?," Proc. IEEE **94,** 911-934 (2006).
2. S. T. Chu, B. E. Little, W. Pan, T. Kaneko, S. Sato, and Y. Kokobun, "An Eight-Channel Add-Drop Filter Using Vertically Coupled Microring Resonators over a Cross Grid," IEEE Photon. Technol. Lett. **11**, 691-693 (1999).
3. E. J. Klein, D. H. Geuzebroek, H. Kelderman, G. Sengo, N. Baker, and A. Driessen, "Reconfigurable Optical Add-Drop Multiplexer Using Microring Resonators," IEEE Photon. Technol. Lett. **17**, 2358-2360 (2005).
4. R. A. Soref, and B. E. Little, "Proposed N-Wavelength M-Fiber WDM Crossconnect Switch Using Active Microring Resonators," IEEE Photon. Technol. Lett. **10**, 1121-1123 (1998).
5. B. E. Little, S. T. Chu, W. Pan, and Y. Kokobun, "Microring resonator arrays for VLSI photonics," IEEE Photon. Technol. Lett. **12**, 323-325 (2000).
6. S. Suzuki, K. Shuto, and Y. Hibino, "Integrated –optic ring resonators with two stacked layers of silica waveguide on Si," IEEE Photon. Technol. Lett. **4,** 1256-1258 (1992).
7. D. Klunder, E. Krioukov, F. S. Tan, T. van der Veen, H. F. Bulthuis, G. Sengo, C. Otto, H. J. W. M. Hoekstra, and A. Driessen, "Vertically and laterally waveguide-coupled cylindrical microresonators in Si_3N_4 on SiO_2 technology," Appl. Phys. B **73**, 603-708 (2001).
8. K. Worhoff, L. T. H. Hilderink, A. Driessen, and P. V. Lambeck, "Silicon oxinitride – a versatile material for integrated optics applications," J. Electrochem. Soc. **149**, F85-F91 (2002).
9. F. C. Blom, D. R. van Dijk, H. J. W. M. Hoekstra, A. Driessen, and Th. J. A. Popma, "Experimental study of integrated-optics microcavity resonators: Toward an all-optical switching device," Appl. Phys. Lett. **71**, 747-749 (1997).
10. B. E. Little, S. T. Chu, A. Haus, J. Foresi, and J.-P. Laine, "Microring resonator channel dropping filters," J. Lightw. Technol. **15**, 998-1005 (1997).
11. D. H. Geuzebroek, E. J. Klein, H. Kelderman, N. Baker, and A. Driessen, "Compact wavelength-selective switch for gigabit filtering in access networks," IEEE Photon. Technol. Lett. **17**, 336-338 (2005).
12. D. H. Geuzebroek, "Flexible Optical Network Components based on Densely Integrated Microring Resonators," PhD Thesis, University of Twente, ISBN 90-365-2258-7, 2005.
13. E. J. Klein, "Densely Integrated Microring-Resonator Based Components for Fibe-To-The-Home Applications," PhD Thesis, University of Twente, ISBN 978-90-365-2495-7, 2007.
14. L. C. Kimerling, D. Ahn, A. B. Apsel, M. Beals, D. Carothers, Y.- K. Chen, T. Conway, D. M. Gill, M. Grove, C.- Y. Hong, M. Lipson, J. Liu, J. Michel, D. Pan, S. S. Patel, A. T. Pomerene, M. Rasras, D. K. Sparacin, K.-Y. Tu, A. E. White and C. W. Wong, "Electronic-photonic integrated circuits on the CMOS platform," Proc. SPIE **6125** (2007).
15. C. K. Madsen, and J. H. Zhao, "Optical Filter Design and Analysis: A Signal Processing Approach," John Wiley & Sons (ISBN: 0-471-18373-3), May 1999.

16. T. Barwicz, M. R. Watts, M. A. Popovic, P. T. Rakich, L. Socci, F. X. Kärtner, E. P. Ippen and H. I. Smith, "Polarization-transparent microphotonic devices in the strong confinement limit," Nature Photonics **1**, 57-60 (2007).

17. D. J. W. Klunder, C. G. H. Roeloffzen, and A. Driessen, "A Novel Polarization-Independent Wavelength-Division-Multiplexing Filter Based on Cylindrical Microresonators," IEEE J. Sel. Top. Quantum. Electron. **8**, 1294-1299 (2002).

18. A. Driessen, D. H. Geuzebroek, E. J. Klein, R. Dekker, R. Stoffer, C. Bornholdt, "Propagation of short lightpulses in microring resonators: Ballistic transport versus interference in the frequency domain," Opt. Commun. **270**, 217-224 (2007).

19. D. H. Geuzebroek E. J. Klein, H. Kelderman, C. Bornholdt, and A. Driessen, "40 Gbit/s Reconfigurable Optical Add-Drop Multiplexer based on Microring Resonators, in *Proceedings of the European Conference on Optical Communications (ECOC)*, 983-986 (2005).

1. Introduction

The application of optical fibers has led to virtually loss-less point to point data links in the core network with practically unlimited bandwidth. In response to increasing bandwidth demands of consumers the optical techniques employed in these networks are now gradually extended towards the consumers premises. At the access network level, where equipment is shared by a few users at the most, cost is the major issue. In addition, the demand of optical transparency at the nodes and hubs, which excludes conversion between the optical and electrical domains, results in a high degree of complexity of the devices. Fortunately, through the use of flexible WDM bandwidth allocation schemes that provide bandwidth where needed [1], and cheap mass-produced densely integrated optical components, the cost can be reduced significantly.
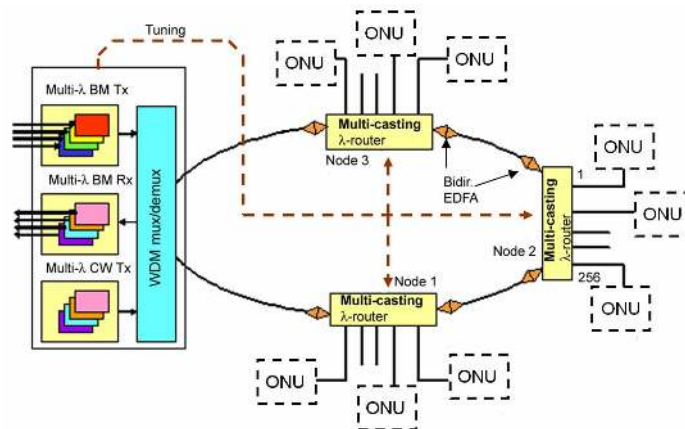

Fig. 1. Reference network architecture.

The components presented in this paper have been designed for use in a (reference) network architecture as shown in Fig. 1. The architecture is based upon a multi-wavelength configuration, using different wavelengths to separate the various services and address upgradeability requirements. Bidirectional communication between the central site and any of the Optical Network Units (ONU) takes place along a single fiber where redundancy is built in by means of a ring topology. The channels in the network, each with a capacity of 1.25 Gbit/s, can be allocated to a single or a group of users via reconfigurable nodes that are controlled from the central node where the various up- and downstream signals are handled.

In this paper the design, fabrication and characterization of two possible implementations of the reconfigurable nodes, a 4-channel reconfigurable Optical Add Drop Multiplexer (rOADM) [2,3] and a 1x4x4 λ-router [4,5], both operating at 1310 nm will be discussed. Also, recent experimental results of a rOADM operating at 1550 nm will be discussed.

2. Design and fabrication

The router as well as the rOADMs have been implemented using vertically coupled Microring Resonators (MRs) [6,7] fabricated in the Si_3N_4/SiO_2 materials system [8]. The application of a high contrast materials system ($\Delta n \approx 0.55$) for the highly selective MR-based filters allows for the creation of complex devices on a small footprint [9-13]. It should noted, however, that the devices reported here could also be realized readily in silicon waveguides using the vertically stacked double silicon-on-insulator photonic system that was reported recently [14]. For such a silicon photonic system, the device architectures would be exactly the same as we have presented here.

The schematic layouts of the rOADM and the λ-router are given in Fig. 2. The rOADM consists of a central bus waveguide which is coupled to four MRs. These resonators can be used to add or drop channels to and from the four add- and drop ports. The input and output of the central bus waveguide are positioned on the same side as the drop ports. This gives the option to use the device as either a reconfigurable de-multiplexer when attached to one- or as an rOADM when attached to two fiber arrays. For the latter option the alignment waveguide indicated in Fig. 2a is then used for alignment of the second fiber array (it has no function in the actual operation of the device). The MRs and port waveguides in the rOADM shown in Fig. 2a are vertically spaced at 250 µm. Although a smaller spacing is possible, this is not practical since the device has been designed to interface with a fiber array with a fiber pitch of 250 µm. Also, a smaller distance will increase the thermal crosstalk between the MRs which, for two MRs 250 µm apart is currently in the order of 0.6 pm/mW of dissipated heater power [12].
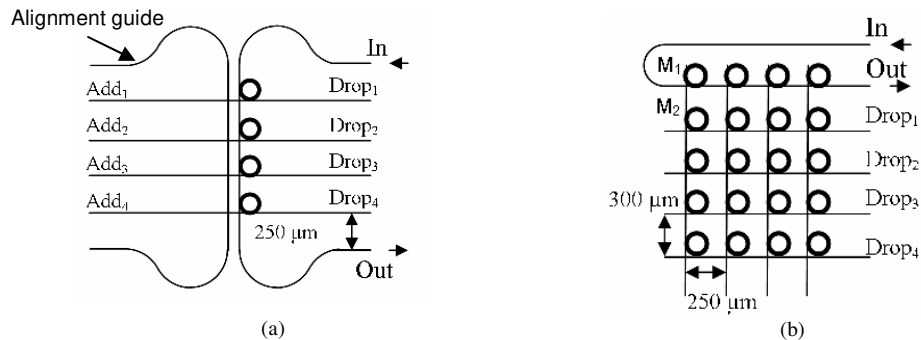

Fig. 2. Schematic layout of an OADM (a) and a λ-router (b) based on microring resonators.

The λ-router in shown in Fig. 2b consists of a single 4-MR de-multiplexer (the upper row) and a 4x4 MR routing matrix. The de-multiplexer consists of four MRs that drop up to four channels from the input port into the columns of the routing matrix. From here, by tuning the resonance wavelength of the MRs in the routing matrix, the channels can be dropped onto the drop ports in any given combination. In the router the vertical spacing between the drop-port waveguides is 300 µm due to the additional space required to place the electrode wires (see Fig. 4b, 13). The horizontal spacing between the MR columns is 250 µm.

The λ-router and the rOADM designs are based on a single MR unit cell design that is copied a certain number of times to create the desired component. The MR cell consists of a ring resonator that is vertically coupled to its port waveguides. Both port waveguides and their crossing lie in the same plane. It is known that the filter- or switching performance of a single MR can be largely improved by implementing higher order filters consisting of 2 or more MRs [15]. In the present case, however, single MR elements only are considered with consequently limited performance. The port waveguides are placed in a cross-grid [5] in order to improve layout efficiency. All the MRs are made thermally tunable by means of a thin-film omega-shaped chromium heater.
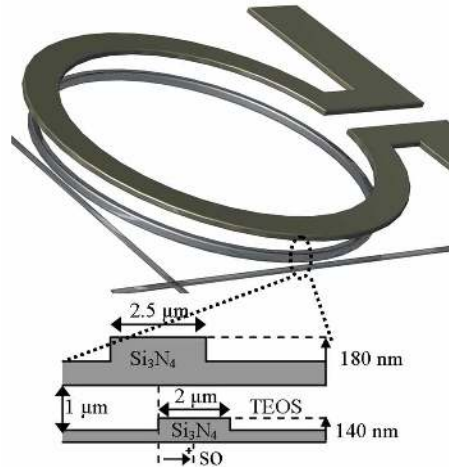
Fig. 3. Top view and coupling region cross-section of the MR unit cell.

A 3D view and a cross-section of the MR unit cell are shown in Fig. 3. The MR has a radius of 50 µm and is realized by reactive ion etching (RIE) of a Si_3N_4 layer with a thickness of 180 nm. The port waveguides are implemented in a Si_3N_4 layer with a thickness of 140 nm. In the devices intended for 1310 nm operation the resonator and port waveguides of the MR are etched down to create ridge waveguides with a ridge height of 90 nm and 80 nm respectively. For operation at 1550 nm the waveguides of the MR are etched through completely. Both designs have been optimized for MR bend loss and coupling of the MR with its port waveguides. It is therefore not possible to use the MR designed to operate at 1550 nm with a wavelength 1310 nm and vice-versa as is the case in some optical devices. In fact, the waveguides designed for operation at 1550 nm would be bi-modal at 1310 nm.

Because of material stress the maximum thickness of the Si_3N_4 layers is about 340 nm. It is therefore not possible to create a resonator waveguide geometry that has polarization independent behavior since the TM mode will typically have a significantly lower effective refractive index and higher losses in MR waveguides with a low aspect ratio. Hence the MRs are optimized for the TE polarization only. It therefore needs to be noted that the devices presented here are ultimately intended to be integrated as part of a device that uses polarization diversity to achieve polarization independence [13,16,17].

A major concern when fabricating vertically coupled MRs [6,7,13] is the correct alignment of the resonator to the port waveguides. An advanced waferstepper tool, in our case an ASML PAS-5500[TM]/275, was therefore used for the exposure of the critical resonator and port waveguide layers. This way an alignment accuracy better than 100 nm could be obtained. For the non critical layers such as the electrodes contact lithography was used in order to reduce the overall processing cost. In Fig. 4 the mask layouts of the rOADM and the λ-router, created from an overlay of the stepper and contact reticle images, are given. As shown a complete λ-router chip measures only 5 mm by 1.8 mm of which the largest part is occupied by the access waveguides and electrodes.
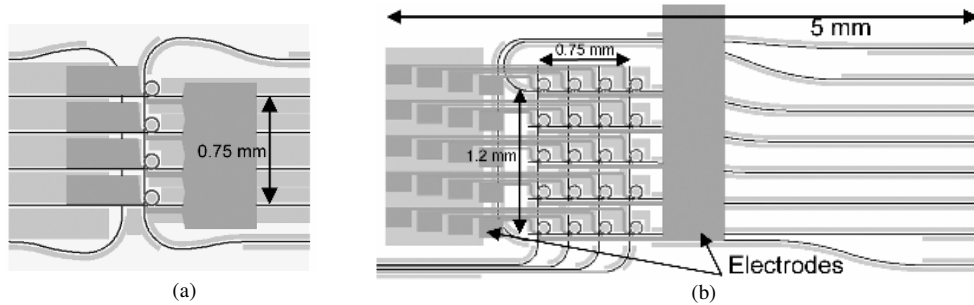
Fig. 4. Mask designs of the rOADM (a) and the λ-Router (b). A complete rOADM chip measures 5 mm by 1.5 mm while the λ-Router is only slightly larger, measuring 5 mm by 1.8 mm.

To facilitate the use of the stepper, 120 nm deep alignment markers were first etched into a bare silicon wafer. These markers are used for alignment in all subsequent exposure steps. The wafer was then thermally oxidized with a resulting oxide thickness of 6 µm. Next a 140 nm thick layer of low pressure chemical vapor deposition (LPCVD) Si_3N_4 (n=1.98) was grown on top [8]. After exposure using the stepper the port waveguides were etched in this layer using RIE. A 1 µm TEOS (tetraethoxysilane) SiO_2 separation layer was deposited next. Because the TEOS layer closely follows the topography of the underlying layers this layer was chemically mechanically polished (CMP). This avoids the "lifting up" of the resonator waveguide on top of the port waveguide, as is shown in the cross-section of an MR fabricated without CMP in Fig. 5, which can significantly increase the MR roundtrip losses.
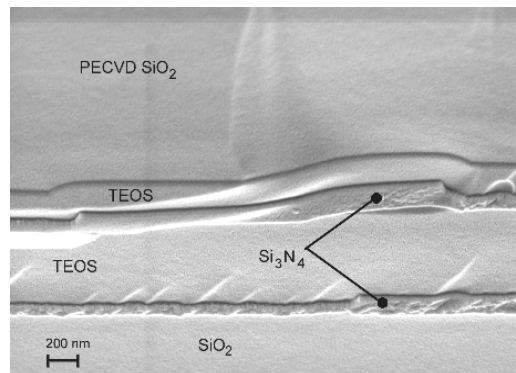

Fig. 5. SEM micrograph of the cross-section of a MR. In this instance no CMP was used on the TEOS separation layer, resulting in a lifting of the MR on top of the port waveguides.

After the CMP step the 180 nm thick Si_3N_4 resonator layer was deposited, exposed with the stepper and etched using RIE. A passivation layer consisting of 0.5 µm TEOS and 3.5 µm plasma enhanced CVD SiO_2 were deposited next after which the device was annealed at 1150°C. On top of this layer stack, of which the individual layers can be discerned in Fig. 5, the heaters are created by sputtering 200 nm of chromium followed by lift-off. Finally, to reduce the resistance of the leads to the heaters, the leads are covered with a 200 nm thick layer of gold by a combination of sputtering and lift-off.

After fabrication some devices were selected for packaging. The packaging not only makes it easier to measure a device but, in the case of the router, is a necessity: only by making wirebonds between the heater electrodes and a carrier substrate - as shown in the inset in Fig. 6 - could all heaters be addressed. Since packaging is a time-consuming and costly

process, only a few devices are packaged into a box that contains the optical chip and all the controlling logic as shown in Fig. 6.
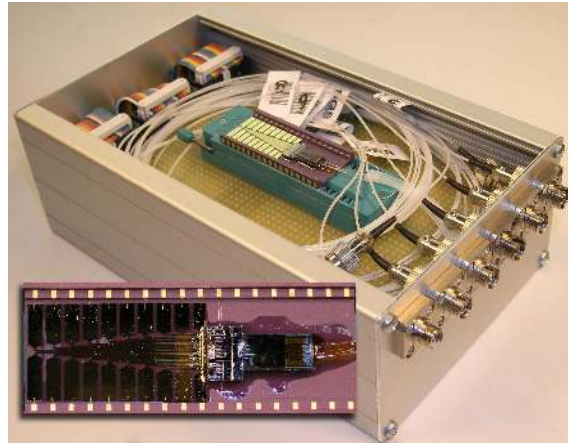

Fig. 6. A λ-router packaged in a box containing all controlling logic. The inset shows a close-up of the pigtailed router chip.

The selection of a device to be packaged is made based on the performance of the individual resonators in the devices. The λ-router and OADM devices are fabricated with a range of MR coupling constants by varying the port waveguide offset *so* (see Fig. 3, the + denotes the positive direction of so) in the designs. This variation results in devices with different performance characteristics (e.g. smaller coupling constants increase the filter selectivity of the MR but also reduce its bandwidth). In the OADM the resonators can be measured individually. For the λ-router, however, this is not possible and test sets of single MRs located near the routers are used. In Fig. 7 the drop responses of a number of resonators in a test set, with offsets *so* between 1.0 µm and 2.0 µm, are given. Also illustrated by these responses is the high uniformity of the fabricated resonators across the wafer. The maximum distance between the resonators in this test set is nearly 5 mm but the maxima of the responses are within 20 pm of each other. In the devices presented in the following sections the decision was made to package the devices with an offset of 1.6 µm as a compromise between bandwidth and filter selectivity.
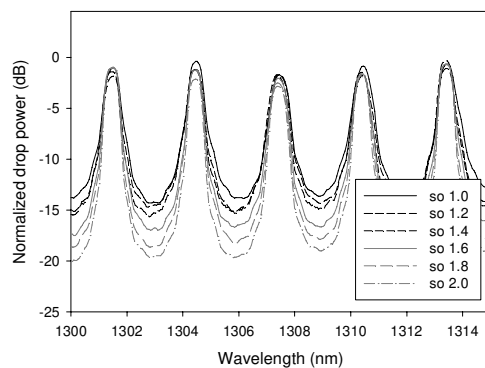

Fig. 7. MR drop response for a number of MR offsets.

3. OADM operating at 1310 nm

The realized 1310 nm rOADM, of which a realized chip is shown in Fig. 8, was measured using a broadband source and an Optical Spectrum Analyzer (OSA) with a resolution of 0.1 nm. Figure 9 shows the normalized responses measured for the four drop ports when the broadband source was connected to the "In" port of the rOADM (see Fig. 2a). To demonstrate the dropping of four different channels to these ports the resonance frequency of each MR in the rOADM has been tuned to a different wavelength. The resonators were tuned by applying a DC voltage up to 7 V across the heaters on top of the MRs. The tuning efficiency is about 7 pm/mW of dissipated heater power. In the drop port responses the effects of channels dropped by adjacent MRs can be observed, for instance in the response at the fourth drop port. The three dips in the response of this port are the through responses of the three preceding MRs. For the drop port responses shown the filter rejection ratio of the individual MRs is ≈16.7 dB. From the measurements the amplitude coupling constants of the individual MRs were determined to be $\kappa_1=\kappa_2=0.40 \pm 0.01$ and the resonator losses 33 ±3 dB/cm. The FSR and Finesse are 3.0 nm and 10.6 respectively, giving a FWHM of 0.28 nm (=46 GHz @1310 nm). The channel crosstalk for channels spaced at 100 GHz (0.6 nm @1300 nm) is ≈-12dB. The considerable losses in the resonator are due to the non-optimized ridge height of the resonator. These losses also resulted in relatively high input to drop port on-chip insertion losses of the resonators of ≈5 dB. As can be seen in Fig. 9 the difference in dropped power between the consecutive drop responses is around 0.6 dB. Of this 0.2 dB can be attributed to power lost in and dropped by preceding MRs. The remaining 0.4 dB is lost in the waveguides between the MRs, including the input to through port insertion loss and the loss at the waveguide crossings.
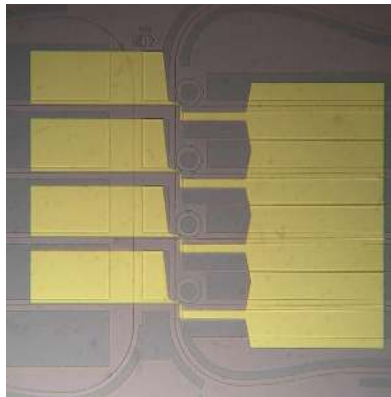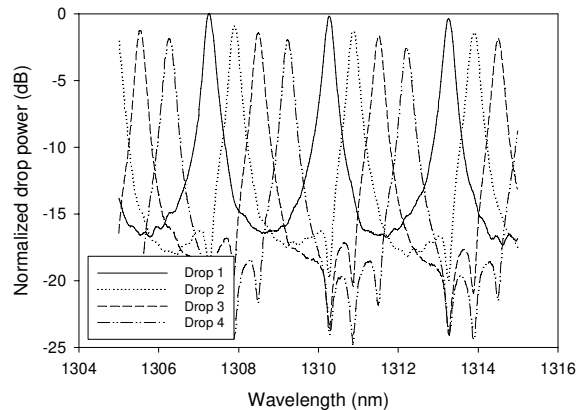

Fig. 8. Photograph of a realized rOADM.

Fig. 9. Drop responses of $Drop_1$ to $Drop_4$ for a broadband source connected to the "In" port.

In addition to the spectral measurements a system level measurement at 1.25 Gbit/s was performed. First, a reference measurement was done using the setup as shown in Fig. 10 (dashed line) in order to find the sensitivity of the receiver. The extinction ratio of the modulator that was used is 7.7 dB at 1305.2 nm. Next, the dropped signal was measured at the $Drop_1$ port of the rOADM. For this purpose the corresponding MR was tuned to drop a signal at 1305.2 nm. As can be seen in the results of the BER measurements (PRBS equal to 2^{31}-1) in Fig. 11 no significant power penalty was measured. The received eye diagrams show no negative influence of the rOADM on the eye parameters, as can be expected from the 46 GHz bandwidth of the MRs [18] that offers the possibility of even higher bitrates [19].
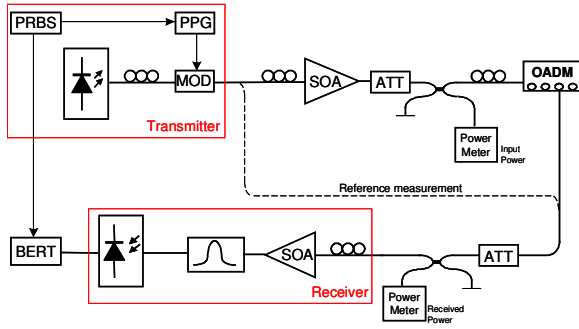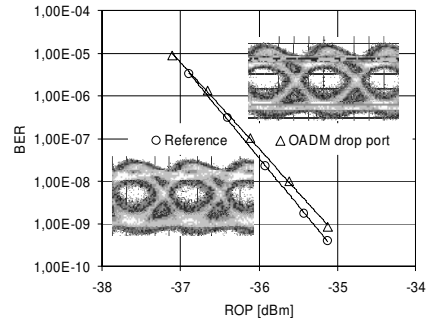
Fig. 10. BER measurement setup.

Fig. 11. BER results and eye diagrams.

4. OADM operating at 1550 nm

The realized 1550 nm rOADM was measured using a HP81689A tunable laser combined with a HP81536A detector. In Fig. 12 the responses measured at the $Drop_1$ and $Drop_2$ port and the OADM through (Out) port are given. All responses were measured at a resolution of 10 pm. Only the MR corresponding to the $Drop_1$ port was tuned for these measurements, resulting in the single sharp dip in the through response. The broader dip in the through response is the combined response of the three untuned MRs.

The measurements show a 23 dB high resonance peak of the drop response and an 18 dB dip in the through response belonging to the first tuned MR. Assuming a symmetrical alignment of the MR to its port waveguides the coupling coefficients and the MR loss can be determined to be $\kappa_1=\kappa_2=0.34 \pm 0.02$ and 4.9 ± 0.5 dB/cm respectively. The FSR of the MR is 4.37 nm and the FWHM is 0.19 nm ($\approx$24 GHz @1550 nm). The Finesse is $\approx$23. The device through port insertion loss including fibers is $\approx$13 dB. This value includes an estimated 5 dB fiber-chip coupling loss per facet and 1 dB on-chip losses.
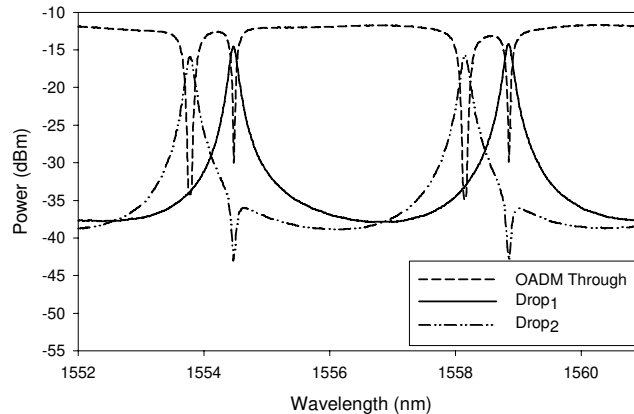

Fig. 12. Measured 1550 nm rOADM responses showing the through response and two drop responses. For the $Drop_1$ port response the heater of the corresponding MR was activated.

5. λ-Router measurements

The λ-router, of which a realized chip is shown in Fig. 13, was characterized before and after packaging. Before packaging only a limited number of heaters could be contacted using probe pins due to the small size of the device. Hence, only the selection and switching of a single channel at a time could be measured. Fig. 14 shows the responses measured at the $Drop_1$ port

for three different tuning configurations of resonators MR1 and MR2 (see Fig. 2b). The measurements of the drop port were made using the OSA with a broadband source connected to the Input port. The first response was measured with all heaters switched off (no tuning). The spectral response of this configuration shows a single broad peak (per FSR) which is caused by the interaction of the resonators in the first and second row of the router that all drop at nearly identical wavelengths. In the second response a single channel was selected by tuning MR1 by half a FSR (1.5 nm). The power dropped by this MR only shows up as a minor peak in the response because it is blocked by MR2. The channel, although selected, is therefore still switched off. However, when MR2 is tuned to the same wavelength as MR1 then full power is dropped on the channel and the channel is effectively switched on. A comparison between the second and third response shows that the "on" / "off" switch ratio in a channel that can be obtained for this λ-router is $\approx$15 dB. The FWHM of the dropped channel is 0.22 nm (=37 GHz @ 1310 nm).

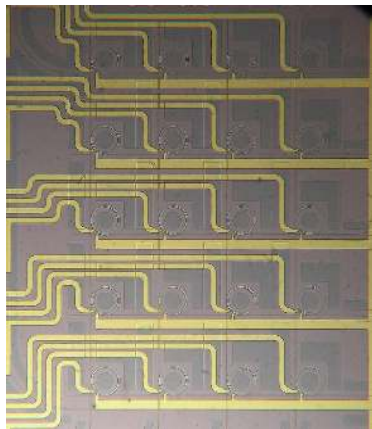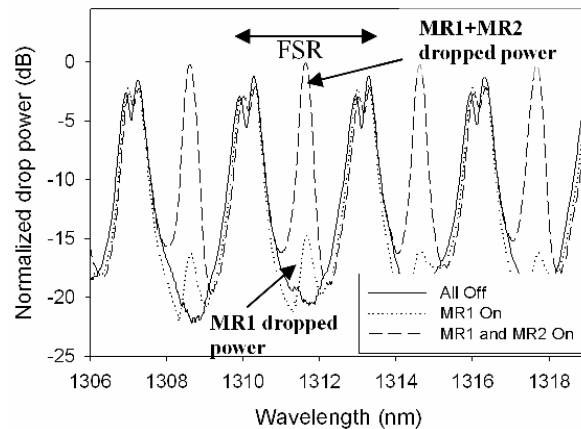

Fig. 13. Realized
1x4x4 λ-router.

Fig. 14. Switching of a single channel in the
router.

After packaging all resonators in the λ-router could be tuned simultaneously, allowing for combinations of channels to be dropped. The measurements in Fig. 15 show the dropping of two and three channels to the Drop$_1$ port. For this measurement respectively two and three MRs in the second row were tuned to a resonance wavelength equal to that of an MR in the top row so that they dropped the channel on the corresponding column to the Drop$_1$ port. Simultaneously the MRs in the second row that did not drop a signal were tuned such that they did not drop the channel present on their column but also were not inadvertently dropping one of the channels already present on the Drop$_1$ port waveguide. By comparing the two measurements it is seen that the on/off ratio of a dropped channel is $\approx$8 dB. The reduction in on/off ratio when compared with the single channel measurement in Fig. 14 is a consequence of the reduced channel spacing of about ¼ of the FSR. Also, due to stability problems with the fiber-chip coupling, the insertion losses increased by 15 dB. This resulted in the measurement being made close to the detection limit of the OSA where higher noise level negatively affects the on/off ratio.
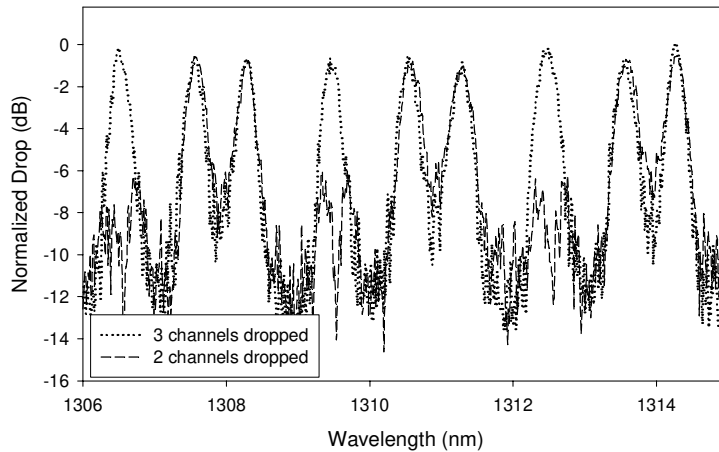
Fig. 15. Responses measured at the $Drop_1$ port of the λ-router when 2 or 3 channels are dropped.

6. Conclusion

A 1x4x4 channel λ-router operating around 1310 nm and two types of reconfigurable 4-channel rOADM, operating around 1310 or 1550 nm have been discussed. The devices are intended for use in access network applications. The 1310 nm OADM was tested at a bitrate of 1.25 Gbit/s without signal degradation and, given the MR bandwidth, even higher bitrates up to 40 Gbit/s can be expected [18,19]. For all devices it has been shown that by means of thermal tuning of the MRs the wavelength channels can be reconfigured. Measurements performed on the router demonstrated its ability to select and switch one or multiple channels to an output. Due to the use of microring resonators these devices were able to integrate complex switching functionality on a small footprint: less than 2 mm^2 for the devices discussed here. These devices therefore have the potential to enable more cost effective solutions for bringing fiber based networks all the way to the consumer.

Acknowledgements